PAPER

Check for updates

Near-infrared high resolution overtone spectroscopy of the hydronium ion H₃O⁺: the $2\nu_3^{2+}$ and $2\nu_3^{2-}$ bands

Chiara Schleif, [ID] Hayley A. Bunn, [ID] Miguel Jiménez-Redondo, [ID] Paola Caselli and Pavol Jusko [ID] *

This work presents the rovibrational spectra of the two strongest first overtone bands of the asymmetric stretching mode ν_3 ($2\nu_3^{2+}$ and $2\nu_3^{2-}$) of the hydronium ion, H₃O⁺. The measurements were performed in a temperature-variable cryogenic 22 pole ion trap using leak-out spectroscopy (LOS), covering an energy range of 6750–6950 cm⁻¹. The spectra were fit with a standard oblate symmetric top Hamiltonian and additional off-diagonal matrix elements accounting for l-doubling to obtain the spectroscopic constants and the band origins, which were determined to be 6845.610(14) cm⁻¹ for $2\nu_3^{2+}$ and 6878.393(13) cm⁻¹ for $2\nu_3^{2-}$.
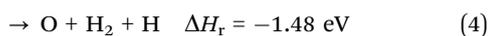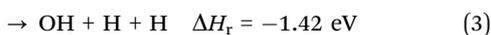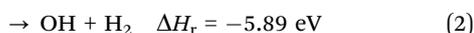
1 Introduction

H₃O⁺ is known to play a fundamental role in interstellar oxygen- and water chemistry.[1,2] It is produced by a well-known reaction chain starting from H₃⁺ and O, followed by subsequent reactions with H₂.[3] H₃O⁺ itself does not react further with H₂ and is eventually destroyed by dissociative recombination (DR)[3,4]

$$H_3O^+ + e^- \rightarrow H_2O + H \quad \Delta H_r = -6.52 \text{ eV} \quad (1)$$

$$\rightarrow OH + H_2 \quad \Delta H_r = -5.89 \text{ eV} \quad (2)$$

$$\rightarrow OH + H + H \quad \Delta H_r = -1.42 \text{ eV} \quad (3)$$

$$\rightarrow O + H_2 + H \quad \Delta H_r = -1.48 \text{ eV} \quad (4)$$
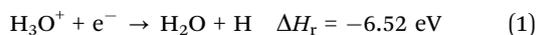
where (1) leads to the production of H₂O (enthalpies of the reaction channels are taken from the active thermochemical tables (ATcT)[5]). The dissociation product OH resulting from channels (2) and (3) can react further *via* the reaction

$$OH + O \rightarrow O_2 + H \quad \Delta H_r = -0.705 \text{ eV} \quad (5)$$

to form O₂.[6] If H₃O⁺ is assumed to be the main precursor of both H₂O and O₂, its detection can be used to make order-of-magnitude predictions of the abundances of the two components,[2] especially when the branching fractions and cross sections of the DR channels are known.[4,7,8]

The DR of H₃O⁺ has been extensively studied in heavy-ion storage rings, *e.g.* with the CRYRING in Stockholm, Sweden or

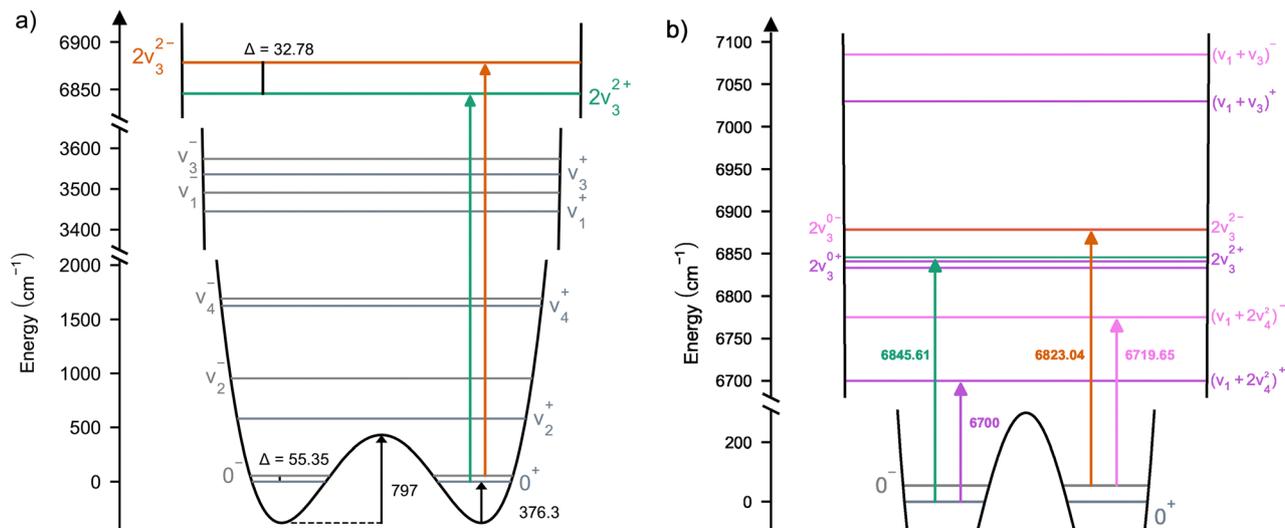ASTRID in Aarhus, Denmark: Neau *et al.*[9] investigated the absolute cross sections of the DR of both H₃O⁺ and D₃O⁺, Jensen *et al.*[4] measured the cross sections of the different channels as a function of energy, and the branching ratios at $E = 0$ for H₃O⁺, HD₂O⁺ and D₃O⁺. Other work focused on individual reaction channels, Andersen *et al.*[7] for instance reported the first observation of the H₂O production path and its branching ratio, while Zhaunerchyk *et al.*[8] investigated the OH formation channel (2). It should be noted that the reported branching ratio of the H₂O production channel differs for all investigations, ranging from 17–18%[9] up to 33%.[7] Further work focusing on deuterated species like D₃O⁺ has been done *e.g.* by Buhr *et al.*[10] using the heavy-ion storage ring TSR in Heidelberg.

The first tentative detection of H₃O⁺ in the ISM was reported by Hollis *et al.*[11] in 1986 towards the Orion-KL nebula *via* a weak single-line detection. The observation was confirmed a few years later by Wootten *et al.*[12] who discovered multiple rotational transitions towards OMC-1 and Sgr B2. In 2006, van der Tak *et al.*[13] mapped H₃O⁺ in Sgr B2 using the APEX telescope. The first detection in the far-infrared through meta-stable rotational transitions of hot H₃O⁺ was reported only much later in 2012 with Herschel in the same source, Sgr B2(N), by Lis *et al.*[14]

In addition to the role of H₃O⁺ in the ISM, the hydronium ion was detected in 2009 by Cassini in the ionosphere of Enceladus, emerging from a cold water plume located in the south polar region.[19] Furthermore, laboratory investigations on exoplanetary atmospheres suggest H₃O⁺ to be a good candidate for future observations targeting the habitability of exoplanets:[20,21] Bourgalais and his team concluded that H₃O⁺ could

Max Planck Institute for Extraterrestrial Physics, Giessenbachstrasse 1, 85748 Garching, Germany. E-mail: pjusko@mpe.mpg.de

This journal is © the Owner Societies 2025

Phys. Chem. Chem. Phys., 2025, **27**, 21307–21314 | **21307**

Fig. 1 Illustrative representations of the inversion potential energy function and vibrational levels of H_3O^+. (a) The potential function expanded by the energy levels of $2\nu_3^{2+}$ and $2\nu_3^{2-}$ identified in this work. The energy levels of fundamentals and ground states were taken from Yu et al.,[15] ground-state inversion splitting from Liu and Oka,[16] ZPE and inversion barrier from Sears et al.[17] The measured transitions are indicated by arrows in the colours of the respective final state. (b) An enlarged representation of the energy range relevant for this work, showing the relative locations of the overtone- and combination bands identified in the ExoMol data.[18] For comparison, the experimentally obtained energy levels of the $2\nu_3^{2+}$ and $2\nu_3^{2-}$ band are included as well. Arrows indicate the allowed transitions from the ground states that are predicted to be most intense. The transition energies show that the $2\nu_3^{2+}$ and $2\nu_3^{2-}$ bands lie close together and well within the measured energy range, while the combination bands are expected rather further away.

be expected in sub-Neptunes[20] and might be one of the most abundant ions in Titan-like atmospheres containing traces of H_2O.[21]

H_3O^+ is a pyramidal symmetric top molecule and isoelectronic to NH_3. Just like ammonia, it can be described by the molecular symmetry group D_{3h} due to its relatively low inversion barrier in the potential energy function[22] which is visualised in Fig. 1(a). This low barrier of 797 cm^{-1} (ref. 17) results in the observed inversion-splitting of all vibrational levels into ± states.

The first experimental high-resolution infrared spectrum of H_3O^+ was measured by Begemann et al.[23] in 1983, including a preliminary analysis of the doubly degenerate asymmetric stretching mode ν_3. Two years later, the group published a more extensive analysis of the same degenerate vibration,[24] reporting strong Coriolis and Fermi interactions between the various modes. Begemann and Saykally[24] observed a large standard deviation of the fit when neglecting those perturbations and concluded that a simultaneous analysis of multiple bands is needed to improve the large residuals. In parallel, Liu et al.[25] reported the observation of both inversion components of the ν_2 band and the rotational and quartic centrifugal distortion constants resulting from a least-squares fit. Based on these measurements they determined the inversion splitting of the ground states to be 55.3462(55) cm^{-1},[16] which is much higher than the value observed for NH_3 (0.8 cm^{-1} (ref. 26)). In 1989, Verhoeve et al.[27] measured the full inversion spectrum between 0^+ and 0^-, observing interactions between states with $\Delta K = \pm 3n$, which they included in the fit to obtain improved spectroscopic constants for the ground states. Tang and Oka[28] investigated the stretching modes ν_1 and ν_3 as well as the

ground states 0^+ and 0^- again after a previous study[29] in great detail in 1999, observing Coriolis interactions and l-type doubling between the stretching modes. They reported rotational and quartic centrifugal distortion constants for all investigated modes and additionally Coriolis coupling and l-doubling constants for ν_3. The first investigations on the doubly degenerate bending mode, ν_4, were published by Gruebele et al.[30] in 1987, where they reported rotational and quartic/sextic centrifugal distortion constants. The group observed significant Coriolis interactions with the ν_2 and $2\nu_2$ levels, but did not consider those perturbations in the fit. More recent work by Yu et al.[15] from 2009 combined previous data of the four fundamental modes and the ground state inversion transition with new measurements of the latter, taking into account the observed strong perturbations by incorporating the Coriolis interaction terms between ν_1 and ν_3 and the $\Delta K = \pm 3$ interactions between the ground states 0^+ and 0^- in their analysis. Inclusion of these coupling terms allowed for an assignment of 200 additional high J-transitions and improved rotational, up to octic centrifugal distortion and Coriolis coupling constants for the ground states and all fundamentals.

While the fundamental modes of H_3O^+ are known in great detail, no rotationally resolved experimental work has been done on its overtones. Only recently, Huang et al.[31] published near-infrared spectroscopy measurements of $H_3O^+ \cdot X_n$ clusters (X = Ar, N_2, CO; n = 1–3) covering the energy region where the first overtones of the stretching modes are expected. They were able to identify several overtone- and combination bands of the ion-tag cluster, but without rotational resolution. Within the ExoMol project,[32] Yurchenko et al.[18] published a thorough theoretical rovibrational molecular line list for H_3O^+, covering

21308 | Phys. Chem. Chem. Phys., 2025, **27**, 21307–21314

This journal is © the Owner Societies 2025

energies up to 10 000 cm^{-1} and temperatures up to 1500 K. The line list is based on an *ab initio* dipole moment surface, an empirical potential energy surface which was globally fitted to the available rovibrational energies of the ground and fundamental vibrational states and variational nuclear motion calculations done with the program TROVE.[33]

In contrast to the hydronium ion, the overtones of NH_3 have been investigated in much greater detail: as an example, Sung *et al.*[34] examined the energy region between 6300–7000 cm^{-1} and assigned over 1000 transitions to seven overtone and combination bands, mentioning the high amount of perturbations observed and expected between the states. In 2020, Furtenbacher *et al.*[35] used the MARVEL database to further expand and improve the accuracy of known rovibrational energy levels in the energy range of up to 7500 cm^{-1}.

The aim of this paper is to gain more knowledge of the first overtones of H_3O^+: this work presents the first high resolution measurements of the strong overtone bands $2\nu_3^{2+}$ and $2\nu_3^{2-}$, two of the first overtones of the doubly degenerate, asymmetric stretching mode ν_3.

2 Experimental details

The measurements of the near-infrared spectrum of H_3O^+ were performed in the CCIT 22 pole cryogenic ion trap, which has been previously described in detail.[36] The H_3O^+ ions (19 *m/z*) were produced in a storage ion source by electron bombardment of a precursor gas mixture consisting of the vapour pressure of H_2O at room temperature (approx. 0.023 atm) topped up with H_2 to 1 atm. The ions extracted from the source were then mass-selected with a quadrupole filter and focused into the trap, where they were decelerated and cooled down with short helium pulses from a piezo valve, obtaining temperatures close to the overall trap temperature. A helium cryostat connected to the trap chamber allows for efficient cooling down to 4 K and enables, in combination with a heating element, flexible temperature regulation. In this experiment, the trap temperature was kept constant at 125 K and 20 K. An Agilent 8164B option 142 light system was used with the module covering 1370–1495 nm, a line width <100 kHz and wavelength-dependent CW power between 1–8 mW. The laser was calibrated using the Bristol 671A wavemeter. To excite a maximum number of ions, the laser was aligned in a triple-pass through the trap cell using a setup of optical mirrors.[37] As the number of ions in the trap is not sufficient to enable the use of direct absorption spectroscopy, action spectroscopy needs to be done instead. In the beginning, it was intended to apply a laser-induced reaction (LIR) scheme using C_2H_4 and C_3H_8 as reaction partners. However, this turned out not to be feasible due to the rapid agglomeration of both neutral species with H_3O^+. Consequently, leak-out spectroscopy (LOS)[38] was chosen to record the overtone spectrum, where N_2 and H_2 were used as neutral buffer gases. The latter was chosen specifically for the measurements at 20 K, below the freezing point of N_2.

The general concept of LOS is described in detail in Schmid *et al.*[38] In brief, the neutral buffer gas N_2 (H_2) is used as collision partner to induce a transfer of the internal energy into kinetic energy, which enables the ions to overcome a potential barrier at the exit and "leak out" of the trap. The potential barrier is tuned in such a way that this process is enhanced when the photon wavelength is on resonance with a rovibrational transition of the H_3O^+ ion, leading to an increase in the observed ion signal. The trapping cycle was set to 3 s (LOS acquisition time around 2.2 s) and a continuous inflow of N_2 (H_2) into the trap chamber throughout the whole measurement cycle resulted in a number density of neutral molecules of around 10^{11} cm^{-3}. Although H_2 is only ∼10% of the mass of H_3O^+, there was no impact on the performance of LOS in comparison to the use of N_2. This further supports the premise, that coupling between vibrational transitions of the two molecules is more important for vibration-transition energy transfer, than the pure momentum conservation due to mass.

An energy range of 1481–1438 nm (corresponding to 6750–6950 cm^{-1}) was scanned in 0.0002–0.0004 nm steps to obtain the spectra reported in this work. Further scanning towards higher and lower energies beyond this energy range within the capacity of the laser did not reveal more transitions. The ExoMol data available for H_3O^+ (ref. 18) that fell into the operation range of the laser module was used to estimate a starting point for the measurements. Every line identified in the scans was re-measured multiple times and the resulting average then used for the line profile and position fit.

For the measurements at 20 K, each transition detected at 125 K was first tested for visibility and then re-scanned to obtain the new line width and intensity at the lower temperature. An exemplary comparison of a line profile visible at both operation temperatures is given in Fig. 2. A change in line width and intensity is clearly evident, although the latter is additionally impacted by the total number of ions in the trap, which can vary significantly between measurements.
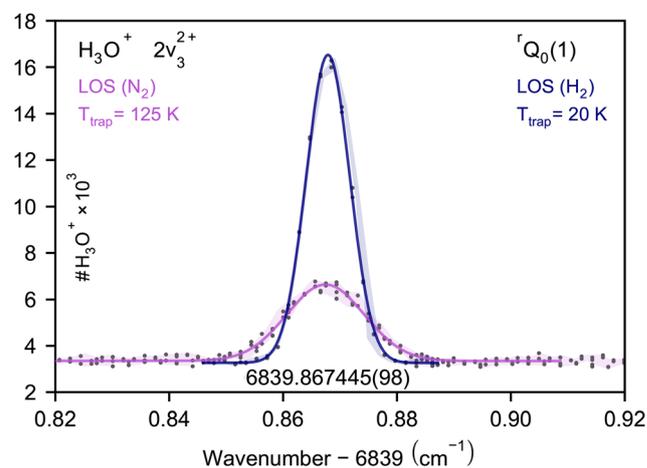

Fig. 2 Comparative representation of a line profile measured at both 125 K (purple) and 20 K (navy). The black number at the bottom of the plot depicts the fitted line position in cm^{-1}, which got assigned to the transition $^rQ_0(1)$ of the $2\nu_3^{2+}$ band. The line profiles at 20 and 125 K were measured with an average of 48 and 235 thousand primary ions in the trap, respectively. Transparent areas in the background represent the std. error around the binned signal (0.002 cm^{-1} bin width).

This journal is © the Owner Societies 2025

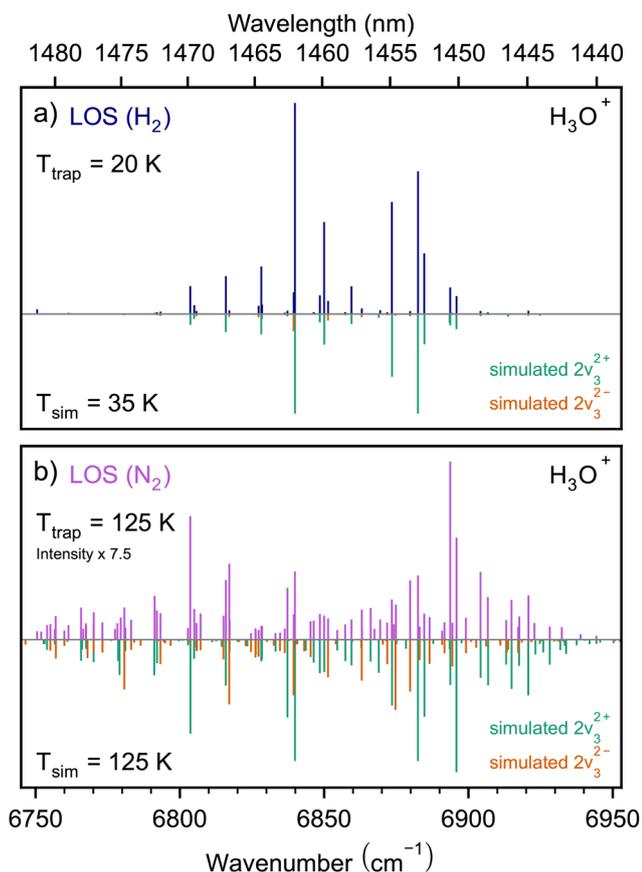*Phys. Chem. Chem. Phys.*, 2025, **27**, 21307–21314 | **21309**

3 Results and discussion

In total, 85 transitions were observed at 125 K, of which 36 are also visible at 20 K. The resulting spectra are shown in Fig. 3 and a complete line list is given in Table S1 in the SI. The spectrum at 125 K was first compared to a refined version of the ExoMol data that contained additional information to the transitions, *i.e.*, initial and final state and the respective TROVE[33] quantum numbers and symmetry labels Γ_{vib} and Γ_{rot} assigned.[18] The quantum numbers given in the data file can be correlated to the normal modes ν_1–ν_4 and the inversion symmetry of the respective state. Together with a comparison to the known overtone- and combination bands of NH_3,[35] this enables an approximate separation of the calculated transitions into the bands that overlap within the energy region. Furthermore, expected values for the angular momentum quantum numbers l_3 and l_4 of degenerate states can be identified. An overview of the theoretically predicted bands separated from the ExoMol dataset is given in Table 1, including an estimation of their band origin where possible. A schematic visualisation of the

Table 1 Selection of theoretically predicted overtone- and combination bands of H_3O^+ in the energy range measured in this work, based on ExoMol[18]

Band[a]	Symmetry	Estim. origin (cm^{-1})
$2\nu_3^{2-}$	E'' [b]	~6879
$2\nu_3^{2+}$	E' [b]	~6841
$2\nu_3^{0-}$	A_2'' [b]	~6878
$2\nu_3^{0+}$	A_1' [b]	~6833
$(\nu_1 + \nu_3)^-$	E'' [b]	~7085
$(\nu_1 + \nu_3)^+$	E' [b]	~7030
$(\nu_1 + 2\nu_4^2)^-$	E'' [b]	~6775
$(\nu_1 + 2\nu_4^2)^+$	E' [b]	~6700
$(\nu_3 + 2\nu_4^2)^-$	E'', A_2'', A_1'' [c,d]	—
$(\nu_3 + 2\nu_4^2)^+$	E', A_1' [c,d]	—
$(\nu_3 + 2\nu_4^0)^\pm$	E [e]	—

[a] Inversion symmetry and vibrational angular momentum quantum numbers l_3, l_4 got assigned based on band symmetry as known for the fundamentals and expected for the overtones based on MARVEL database entries of NH_3.[35] [b] Based on MARVEL database entries of NH_3[35] and confirmed by the ExoMol data. [c] Based on MARVEL database entries of NH_3[35] but no direct confirmation with the ExoMol data possible. [d] Expected splitting based on MARVEL database entries of NH_3.[35] [e] Based on Sung *et al.*[34] but no direct confirmation with the ExoMol data possible.

relative positions of the involved states is given in Fig. 1 in panel (b). Based on the intensity distribution among the bands seen in the ExoMol data file, the strongest bands in the observed energy range appear to be $2\nu_3^{2+}$ and $2\nu_3^{2-}$, with some transitions of the combination bands $(\nu_1 + 2\nu_4)^\pm$ and $(\nu_3 + 2\nu_4)^\pm$ having comparable intensities as the weaker transitions of the $2\nu_3^{2\pm}$ bands. However, it is important to note that the refined version of the dataset only corresponds to a temperature of 300 K, *i.e.*, the intensity distribution will differ at 125 K. Additional factors in the experiment relating to the collision process can lead to variations in the intensities, thereby line assignments based exclusively on intensity are unreliable and should be avoided. The best match was obtained when comparing the measurements to the separated, theoretically predicted $2\nu_3^{2+}$ and $2\nu_3^{2-}$ bands, which raised the assumption that the majority of the measured transitions belong to either one of these two. While the pattern of the predicted subbranches was consistent with the measurements, single line positions did not agree (the comparison is visualised in Fig. S1 in the SI). A detailed analysis of the measured spectrum was, therefore, done using the program PGOPHER,[39] a versatile tool to fit and simulate molecular spectra. The rotational Hamiltonian used for symmetric tops[39] (only including the spectroscopic constants that could be fit in this work) is

$$\begin{aligned}
H_{rot} = {} & \text{Origin} + BN(N+1) + (C-B)K^2 \\
& + \left(-2C\zeta + \eta_J N(N+1) + \eta_K K^2\right) lK \\
& - D_J N^2 (N+1)^2 - D_{JK} N(N+1)K^2 - D_K K^4 \\
& + H_J N^3 (N+1)^3 + H_K K^6,
\end{aligned} \quad (6)$$

where B and C are rotational constants, D and H quartic and sextic distortion constants, and ζ and η Coriolis coupling

Fig. 3 Comparison of the measured and simulated overtone spectrum of H_3O^+ at 20 K (panel (a)) and 125 K (panel (b), scaled by factor 7.5 relative to panel (a) for comparability). The measurements cover an energy range of 6750–6950 cm^{-1}. The simulations were obtained by fitting a Hamiltonian to 68 of the 85 transitions, where 39 transitions got assigned to the $2\nu_3^{2+}$ band (simulation in teal), the other 29 transitions to the $2\nu_3^{2-}$ band (simulation in orange). The resulting parameters are listed in Table 2. For further details see text.

21310 | *Phys. Chem. Chem. Phys.*, 2025, **27**, 21307–21314

This journal is © the Owner Societies 2025

constants. The off-diagonal matrix element included to account for the l-doubling in this case is

$$\langle N, K + 2, l + 1 | H | N, K, l - 1 \rangle$$

$$= \frac{1}{2} q_{+} [(N(N+1) - K(K-1))(N(N+1) - K(K+1))]^{\frac{1}{2}}$$

$$(7)$$

with the l-doubling constant q_{+}. Similar to NH_3, only states with the symmetries A_2', A_2'', E' and E'' are allowed for H_3O^+. The statistical weights of states with A_1' and A_1'' symmetry are zero, as can be derived by nuclear spin statistics described by Bunker and Jensen.[22] In this context, the only difference between NH_3 and H_3O^+ is the nuclear spin quantum number I of the central atom ($= 1$ for ^{14}N and 0 for ^{16}O), which results in the representation Γ_{spin} being a factor of 3 higher for NH_3. The forbidden and allowed state symmetries as well as the relations between the statistical weights are, therefore, identical for both molecules.

The molecular constants of the ground states 0^+ and 0^- obtained by Yu et al.[15] (listed in Table S2 in the SI) were used as initial states to predict the transitions, also considering the $\Delta K = \pm 3$ interaction between the two states by including the off-diagonal matrix elements

$$\langle N, K \pm 3, l | J_z J_{\pm}^{3} | N, K, l \rangle$$

$$= \sqrt{2} \alpha \times (2K \pm 3) \sqrt{ \begin{array}{l} (N(N+1) + (-K \mp 1)(K \pm 2)) \times \\ (N(N+1) + (-K \mp 2)(K \pm 3)) \times \\ (N(N+1) - K(K \pm 1)) \end{array} }$$

$$(8)$$

with $\sqrt{2} \alpha = 8.506$ MHz $\equiv 0.0002837$ cm^{-1}. Linear extrapolations of the spectroscopic constants for the fundamentals ν_3^+ and ν_3^- obtained by the same work[15] (listed in Table S2 in the SI) were used as an initial prediction for the simulation of the overtones.

The two overtone bands $2\nu_3^{2+}$ and $2\nu_3^{2-}$ are known from NH_3 to be perpendicular (E'/E'' symmetry) and therefore require a conservation of state symmetry.[34] $2\nu_3^{2+}$ is, therefore, excited from the 0^+ and $2\nu_3^{2-}$ from the 0^- ground state. Referring to the predictions from ExoMol,[18] it was evident that the two bands are overlapping heavily, which made a reliable assignment difficult for the majority of the transitions. Consequently, the spectrum was re-measured at 20 K to depopulate the 0^- ground state almost completely and thus minimize transitions owing to the $2\nu_3^{2-}$ band. The resulting spectrum is seen in Fig. 3(a). The $2\nu_3^{2+}$ band was fit using the remaining visible transitions and later refined by stepwise assignment of increasing J transitions from the 125 K spectrum that showed residuals below 0.1 cm^{-1} (in this work, the term "residuals" refers to the difference between experimental line position obtained from the line profile fitting and simulated line position). Some transitions could not be fit although they were assigned reliably. They stayed with a higher deviation and were, consequently, excluded from the fit and marked with * in Table S1 in the SI. The remaining transitions in the 125 K spectrum were assigned to the $2\nu_3^{2-}$

band, which was then fit in a similar procedure. The transitions predicted at 35 K, resulting from the fit at 125 K, well reproduced the observed transitions visible at 20 K as visualised in Fig. 3(a). This provided further confidence in the fit of the two bands. Even though the temperature of the trap chamber was measured to be 20 K, the ions are expected to be slightly warmer, which is confirmed by comparing the simulated spectra at 20 K and 35 K. Around 125 K, the slight temperature difference between ions and trap chamber has a negligible effect on the simulated spectrum. Consequently, the simulation set to the experimental temperature reproduces the spectrum well, as can be seen in Fig. 3(b).

In total, 77 of the 85 measured transitions could be assigned to the two overtone bands, of which 68 were included for the fitting procedures (39 transitions for $2\nu_3^{2+}$, 29 for $2\nu_3^{2-}$). The exclusion of 8 transitions was due to large remaining shifts as explained above. One of the transitions could be assigned certainly only at 20 K, while several assignments became possible at 125 K. This transition was, therefore, not included in the fit either. All assignments are listed in Table S1 in the SI. The 8 transitions that remain unassigned are expected to either belong to another band, e.g., $(\nu_1 + 2\nu_4^2)^{\pm}$, or are perturbed so heavily that no certain assignment is possible.

Ho et al.[29] reported for the bands $\nu_3^{\pm} \leftarrow 0^{\pm}$ that ^{P}P-transitions of $J'' = 4, 5, 7, 8$ ($\nu_3^+ \leftarrow 0^+$) and $J'' = 4, 5, 8, 12$ ($\nu_3^- \leftarrow 0^-$) showed large residuals and had to be excluded from the fit. The group was able to prove that the deviations are expected to be caused by perturbations, but its source could not be determined. Tang and Oka[28] extended the assignment of the $\nu_3^{\pm} \leftarrow 0^{\pm}$ bands to higher J, K transitions: they observed an increase in the residuals proportional to J–K, specifically for ^{P}P-transitions with $K' \geq 7$.

Of the 77 transitions assigned in this work, 18 turn out to be ^{P}P-transitions, and only 4 of the 8 heavily shifted transitions. A pattern within the residuals of this type of transition could, therefore, not be determined reliably. Instead, the analysis focuses on patterns in the upper state quantum numbers J' and K'.

The majority of the transitions got assigned to $J' = 2, 3, 4$ and $K' = 0, 1, 2, 3$. 10 transitions got assigned to $J' = 5$ and 2 to $J' = 6$. No transitions with J' and $K' > 7$ have been observed. Only one transition got assigned to $J', K' = 7$. In regard of $|J - K|$, 36 transitions show $|J - K| = 0$, 21 $|J - K| = 1$, 13 $|J - K| = 3$ and only 2 $|J - K| = 4$, both belonging to $J' = 4$. A comparison of the change in residuals with increasing $|J - K|$ for $J' = 4$ did not reveal any proportional trend as it was seen for higher J' for $\nu_3^{\pm}$ by Tang and Oka.[28] In general, for the 8 heavy shifted transitions, no pattern could be identified within the involved J' and K' states. The only apparent aspect is that solely $J', K' = 3, 4, 5$ seem to be sufficiently affected. When looking at transitions with residuals > 0.01 cm^{-1}, it becomes evident that especially transitions with $J' = 3$ show larger deviations, while $J' < 3$ are less affected. Higher J' transitions are seen at both higher and lower residuals, so no clear pattern can be drawn.

A trend in the deviations is expected to become clearer when transitions with higher J' and K' are incorporated. This

This journal is © the Owner Societies 2025

Phys. Chem. Chem. Phys., 2025, 27, 21307–21314 | 21311

Table 2 Spectroscopic constants obtained for the overtone bands $2\nu_3^{2+}$ and $2\nu_3^{2-}$ of H_3O^+, values given in cm^{-1} with 1σ in parentheses

Parameter	$2\nu_3^{2+}$	$2\nu_3^{2-}$
Origin	6845.610(14)	6878.393(13)
B	10.8905(43)	10.7716(25)
C	6.1091(36)	6.1851(47)
D_J	0.00173(33)	0.00024(11)
D_{JK}	−0.00318(23)	−0.00171(32)
D_K	0.00265(39)	0.00296(40)
ζ	0.03784(47)	0.02813(70)
η_J	−0.00303(53)	0.0064(11)
η_K	0.00524(50)	−0.0028(11)
q_+	0.2099(18)	−0.2239(16)
$H_J \times 10^5$	3.24(76)	0.0
$H_K \times 10^5$	−3.71(94)	5.33(60)

assumption is supported by Tang and Oka,[28] where clear trends are observed especially for $K' \geq 7$. No such transitions were measured within this work, as the line intensities are expected to be significantly weaker and therefore not visible with this experimental setup.

The spectroscopic constants obtained from the fit of $2\nu_3^{2+}$ and $2\nu_3^{2-}$ are listed in Table 2, including 1σ uncertainty in the last two significant digits in parentheses. Apart from H_J (and H_K for $2\nu_3^{2+}$), no higher distortion constants could be fit with reasonable errors, which is why they were put to zero, likely due to the lack of transitions to higher J' and K' states. Despite excluding the largest deviations from the fit, many line positions remain shifted with respect to the simulations, as can be seen in Table S1 in the SI. The best fit of the $2\nu_3^{2+}$ band has an average error of 0.0265 cm^{-1}, the $2\nu_3^{2-}$ band 0.0147 cm^{-1}. The main cause of this is expected to be some strong perturbations caused by the bands predicted nearby, visualised in Fig. 1. In the past, strong Coriolis and Fermi interactions with neighbouring bands were not only seen for the fundamentals, described *e.g.* by Tang and Oka[28] and Yu *et al.*,[15] but also for the fundamental, combination and overtone bands of NH_3 (described *e.g.* in Sung *et al.*[34]). Therefore, similar interactions are also expected for the overtone and combination bands of H_3O^+. Since the two bands identified in this work are separated by only 32.78 cm^{-1} and have both E'/E'' symmetry, they are prone to perturb each other through Fermi interaction. Attempts at implementing this interaction and also perturbation by unobserved states were not successful and did not obtain a meaningful improvement of the residuals. An effective fit to unperturbed transitions is, therefore, reported here. It is expected that inclusion of higher J' transitions will assist in correctly modelling the interactions responsible for the deviations. In fact, Yu *et al.*[15] reported that considering the strong Coriolis interactions between the fundamental stretching modes ν_1 and ν_3 and inclusion of 200 more high-J transitions enabled an improvement of the molecular parameters and frequency predictions of further high-J transitions. Furthermore, gaining information about the unobserved nearby states is required to treat the interaction in the fits. The combination bands $(\nu_1 + 2\nu_4)^{\pm}$ are, according to the ExoMol predictions, expected to be the next most intense bands nearby the measured energy region and could play an important role in the

observed perturbations. To further investigate these assumptions, more measurements are needed, covering the energy range of the bands predicted nearby and sensitive to significantly weaker transitions. For this, a different laser light source would be needed.

4 Conclusions

In this work, the two degenerate overtone bands $2\nu_3^{2+}$ and $2\nu_3^{2-}$ have been identified and fit using a standard oblate symmetric top Hamiltonian to obtain two sets of spectroscopic constants, including rotational, centrifugal distortion, Coriolis coupling and l-type doubling constants. Apart from H_J and H_K, no higher order centrifugal distortion constants could be obtained. Although interaction between the identified bands and severe perturbations by unobserved nearby bands were observed, no interaction parameters could be determined and therefore only the effective fits to unperturbed transitions are reported. The identification of further combination- and overtone bands, *e.g.* $(\nu_1 + 2\nu_4)^{\pm}$, is expected to facilitate the implementation of perturbation terms, together with additional measurements of higher J-state transitions for $2\nu_3^{2+}$ and $2\nu_3^{2-}$. Such measurements are also expected to enable the determination of higher centrifugal distortion constants.

In comparison with the high-resolution measurements obtained in this work, the calculations from ExoMol[18] are in agreement regarding subbranch structure and separation, but disagree at the level of rotational resolution and therefore prevent a direct line assignment. The theoretical band origins deviate in the order of cm^{-1}, with the prediction of $2\nu_3^{2-}$ being close to the experimental value, while $2\nu_3^{2+}$ shows a slightly higher deviation. Running a cross-correlation between the transitions separated from the ExoMol data and from the experiment showed that a shift to the band origin alone cannot successfully align all rotational transitions at once (see Fig. S2 in the SI). It is, therefore, expected that there are further factors involved to cause the disagreement between predictions and experiment. A fit to the experimental transitions as done in this work is, consequently, essential to provide improved rotational line positions.

As the calculations from ExoMol refer to 300 K, while the measurements were done at 125 K, the simulated spectra were additionally extended to 300 K (using the obtained spectroscopic constants listed in Table 2) in order to match the ExoMol data temperature. The comparison is shown in Fig. S3 in the SI. The agreement of several transitions is again improved when shifting the band origin of the ExoMol calculations, but, similar to the comparison with the experimental data, no alignment of all transitions can be obtained. It is, therefore, to be expected that the fit to the experimental transitions obtained in this work already improves the predictions of higher J and K transitions, despite neglecting the observed perturbations.

Besides supporting the improvement of theoretical calculations, the spectroscopic data obtained in this work is expected to have a wide range of possible applications, as cheap

21312 | *Phys. Chem. Chem. Phys.*, 2025, **27**, 21307–21314

This journal is © the Owner Societies 2025

telecommunication equipment covering the E and S-band can now be used for *in situ* monitoring in emission or absorption. This directly allows for further investigation of the dissociative recombination of H_3O^+ in plasma discharge, the use of spectroscopic identification instead of mass spectrometry in breath analysis,[40] or its detection in hot environments like exoplanetary atmospheres.

Conflicts of interest

There are no conflicts to declare.

Data availability

Supplementary information is available. See DOI: https://doi.org/10.1039/d5cp03187g.

Data for this article, including raw measurements, postprocessing scripts, line lists, and, pgopher file are available at Zenodo at https://doi.org/10.5281/zenodo.14645564.

Acknowledgements

Notes and references

1 E. Herbst and W. Klemperer, *Astrophys. J.*, 1973, **185**, 505–534, DOI: 10.1086/152436.

2 T. G. Phillips, E. F. van Dishoeck and J. Keene, *Astrophys. J.*, 1992, **399**, 533, DOI: 10.1086/171945.

3 E. Herbst, *Chem. Soc. Rev.*, 2001, **30**, 168–176, DOI: 10.1039/A909040A.

4 M. J. Jensen, R. C. Bilodeau, C. P. Safvan, K. Seiersen, L. H. Andersen, H. B. Pedersen and O. Heber, *Astrophys. J.*, 2000, **543**, 764, DOI: 10.1086/317137.

5 B. Ruscic, R. E. Pinzon, G. von Laszewski, D. Kodeboyina, A. Burcat, D. Leahy, D. Montoy and A. F. Wagner, *J. Phys.: Conf. Ser.*, 2005, **16**, 561, DOI: 10.1088/1742-6596/16/1/078.

6 J. Davidsson and L. G. Stenholm, *Astron. Astrophys.*, 1990, **230**, 504–508.

7 L. H. Andersen, O. Heber, D. Kella, H. B. Pedersen, L. Vejby-Christensen and D. Zajfman, *Phys. Rev. Lett.*, 1996, **77**, 4891–4894, DOI: 10.1103/PhysRevLett.77.4891.

8 V. Zhaunerchyk, W. D. Geppert, S. Rosén, E. Vigren, M. Hamberg, M. Kamińska, I. Kashperka, M. af Ugglas, J. Semaniak, M. Larsson and R. D. Thomas, *J. Chem. Phys.*, 2009, **130**, 214302, DOI: 10.1063/1.3141434.

9 A. Neau, A. Al Khalili, S. Rosén, A. Le Padellec, A. M. Derkatch, W. Shi, L. Vikor, M. Larsson, J. Semaniak, R. Thomas, M. B. Någård, K. Andersson, H. Danared and M. af Ugglas, *J. Chem. Phys.*, 2000, **113**, 1762–1770, DOI: 10.1063/1.481979.

10 H. Buhr, J. Stützel, M. B. Mendes, O. Novotný, D. Schwalm, M. H. Berg, D. Bing, M. Grieser, O. Heber, C. Krantz, S. Menk, S. Novotny, D. A. Orlov, A. Petrignani, M. L. Rappaport, R. Repnow, D. Zajfman and A. Wolf, *Phys. Rev. Lett.*, 2010, **105**, 103202, DOI: 10.1103/PhysRevLett.105.103202.

11 J. M. Hollis, E. B. Churchwell, E. Herbst and F. C. De Lucia, *Nature*, 1986, **322**, 524–526, DOI: 10.1038/322524a0.

12 A. Wootten, J. G. Mangum, B. E. Turner, M. Bogey, F. Boulanger, F. Combes, P. J. Encrenaz and M. Gerin, *Astrophys. J. Lett.*, 1991, **380**, L79, DOI: 10.1086/186178.

13 F. F. van der Tak, A. Belloche, P. Schilke, R. Güsten, S. Philipp, C. Comito, P. Bergman and L.-Å. Nyman, *Astron. Astrophys.*, 2006, **454**, L99–L102, DOI: 10.1051/0004-6361:20065289.

14 D. C. Lis, P. Schilke, E. A. Bergin, M. Emprechtinger and the HEXOS Team, *Philos. Trans. R. Soc., A*, 2012, **370**, 5162–5173, DOI: 10.1098/rsta.2012.0025.

15 S. Yu, B. J. Drouin, J. C. Pearson and H. M. Pickett, *Astrophys. J., Suppl. Ser.*, 2008, **180**, 119, DOI: 10.1088/0067-0049/180/1/119.

16 D.-J. Liu and T. Oka, *Phys. Rev. Lett.*, 1985, **54**, 1787–1789, DOI: 10.1103/PhysRevLett.54.1787.

17 T. J. Sears, P. R. Bunker, P. B. Davies, S. A. Johnson and V. Spirko, *J. Chem. Phys.*, 1985, **83**, 2676–2685, DOI: 10.1063/1.449270.

18 S. N. Yurchenko, J. Tennyson, S. Miller, V. V. Melnikov, J. O'Donoghue and L. Moore, *Mon. Not. R. Astron. Soc.*, 2020, **497**, 2340–2351, DOI: 10.1093/mnras/staa2034.

19 R. L. Tokar, R. E. Johnson, M. F. Thomsen, R. J. Wilson, D. T. Young, F. J. Crary, A. J. Coates, G. H. Jones and C. S. Paty, *Geophys. Res. Lett.*, 2009, **36**, L13203, DOI: 10.1029/2009GL038923.

20 J. Bourgalais, N. Carrasco, Q. Changeat, O. Venot, L. Jovanović, P. Pernot, J. Tennyson, K. L. Chubb, S. N. Yurchenko and G. Tinetti, *Astrophys. J.*, 2020, **895**, 77, DOI: 10.3847/1538-4357/ab8e2d.

21 J. Bourgalais, N. Carrasco, Y. Miguel, O. Venot and P. Pernot, *Astron. Astrophys.*, 2021, **654**, A171, DOI: 10.1051/0004-6361/202141328.

22 P. R. Bunker and P. Jensen, *Molecular Symmetry and Spectroscopy*, National Research Council, Canada, 2nd edn, 2006.

23 M. H. Begemann, C. S. Gudeman, J. Pfaff and R. J. Saykally, *Phys. Rev. Lett.*, 1983, **51**, 554–557, DOI: 10.1103/PhysRevLett.51.554.

24 M. H. Begemann and R. J. Saykally, *J. Chem. Phys.*, 1985, **82**, 3570–3579, DOI: 10.1063/1.448914.

25 D. Liu, N. N. Haese and T. Oka, *J. Chem. Phys.*, 1985, **82**, 5368–5372, DOI: 10.1063/1.448620.

26 W. E. Good, *Phys. Rev.*, 1946, **70**, 213–218, DOI: 10.1103/PhysRev.70.213.

27 P. Verhoeve, M. Versluis, J. Ter Meulen, W. Meerts and A. Dymanus, *Chem. Phys. Lett.*, 1989, **161**, 195–201, DOI: 10.1016/S0009-2614(89)87059-9.

This journal is © the Owner Societies 2025

Phys. Chem. Chem. Phys., 2025, **27**, 21307–21314 | 21313

28 J. Tang and T. Oka, *J. Mol. Spectrosc.*, 1999, **196**, 120–130, DOI: **10.1006/jmsp.1999.7844**.

29 W. Ho, C. Pursell and T. Oka, *J. Mol. Spectrosc.*, 1991, **149**, 530–541, DOI: **10.1016/0022-2852(91)90308-W**.

30 M. Gruebele, M. Polak and R. J. Saykally, *J. Chem. Phys.*, 1987, **87**, 3347–3351, DOI: **10.1063/1.453029**.

31 Q.-R. Huang, K. Yano, Y. Yang, A. Fujii and J.-L. Kuo, *Phys. Chem. Chem. Phys.*, 2024, **26**, 10757–10768, DOI: **10.1039/D4CP00458B**.

32 J. Tennyson and S. N. Yurchenko, *Mon. Not. R. Astron. Soc.*, 2012, **425**, 21–33, DOI: **10.1111/j.1365-2966.2012.21440.x**.

33 S. N. Yurchenko, W. Thiel and P. Jensen, *J. Mol. Spectrosc.*, 2007, **245**, 126–140, DOI: **10.1016/j.jms.2007.07.009**.

34 K. Sung, L. R. Brown, X. Huang, D. W. Schwenke, T. J. Lee, S. L. Coy and K. K. Lehmann, *J. Quant. Spectrosc. Radiat. Transfer*, 2012, **113**, 1066–1083, DOI: **10.1016/j.jqsrt.2012.02.037**.

35 T. Furtenbacher, P. A. Coles, J. Tennyson, S. N. Yurchenko, S. Yu, B. Drouin, R. Tóbiás and A. G. Császár, *J. Quant. Spectrosc. Radiat. Transfer*, 2020, **251**, 107027, DOI: **10.1016/j.jqsrt.2020.107027**.

36 P. Jusko, M. Jiménez-Redondo and P. Caselli, *Mol. Phys.*, 2024, **122**, e2217744, DOI: **10.1080/00268976.2023.2217744**.

37 M. Jiménez-Redondo, L. Uvarova, P. Dohnal, M. Kassayová, P. Caselli and P. Jusko, *ChemPhysChem*, 2024, **25**, e202400106, DOI: **10.1002/cphc.202400106**.

38 P. C. Schmid, O. Asvany, T. Salomon, S. Thorwirth and S. Schlemmer, *J. Phys. Chem. A*, 2022, **126**, 8111–8117, DOI: **10.1021/acs.jpca.2c05767**.

39 C. M. Western, *J. Quant. Spectrosc. Radiat. Transfer*, 2017, **186**, 221–242, DOI: **10.1016/j.jqsrt.2016.04.010**.

40 P. Španěl, A. Spesyvyi and D. Smith, *Anal. Chem.*, 2019, **91**, 5380–5388, DOI: **10.1021/acs.analchem.9b00530**.

21314 | *Phys. Chem. Chem. Phys.*, 2025, **27**, 21307–21314

This journal is © the Owner Societies 2025